Pathogenic Aβ A2V versus protective Aβ A2T mutation: early stage aggregation and membrane interaction.

Laura Colombo[1], Alessio Gamba[2], Laura Cantù[2], Mario Salmona[1], Fabrizio Tagliavini[3], Valeria Rondelli[2], Elena Del Favero[2*], Paola Brocca[2]

[1]Department of Molecular Biochemistry and Pharmacology, IRCCS Istituto di Ricerche Farmacologiche "Mario Negri", Via La Masa 19, 20156, Milan, Italy
[2]Department of Medical Biotechnology and Translational Medicine, University of Milan, V.le F.lli Cervi 93, 20090 Segrate, Italy
[3]Neurology V & Neuropathology, IRCCS Foundation "Carlo Besta" Neurological Institute, Via Celoria 11, 20133 Milan, Italy

*Corresponding author:

Elena Del Favero

Dept. of Medical Biotechnologies and Traslational Medicine,

University of Milano,

LITA, Via F.lli Cervi 93

20090 Segrate,

Italy

+39 0250330351

elena.delfavero@unimi.it

Abstract

We investigated the effects of punctual A-to-V and A-to-T mutations in the amyloid precursor protein APP, corresponding to position 2 of Aβ1–42. Those mutations had opposite effects on the onset and progression of Alzheimer Disease, the former inducing early AD pathology and the latter protecting against the onset of the disease. We applied Static and Dynamic Light Scattering and Circular Dichroism, to study the different mutants in the early stages of the aggregation process, essential for the disease. Comparative results showed that the aggregation pathways differ in the kinetics and extent of the process, in the size of the aggregates and in the evolution of the secondary structure, resulting in fibrils of different morphology, as seen by AFM. Mutated peptides had comparable toxic effects on N2a cells. Moreover, as assessed by X-ray scattering, all of them displayed disordering effects on the internal structure of mixed phospholipids-gangliosides model membranes.

Keywords Aβ1-42 peptide; A2V; A2T; Aβ aggregation; Aβ membrane interaction; laser Light Scattering; X-ray Scattering.

1. Introduction

The mechanisms underlying Alzheimer disease (AD) are not yet completely clear but genetic, pathological and biochemical aspects are at the basis of the onset and development of this pathology. In particular, the generation and accumulation of β-amyloid (Aβ) peptides, proteolytic fragments of the membrane-associated amyloid precursor protein (APP), represent a crucial aspect in the manifestation of this pathology [1]. Aβ peptides are extracellularly released in the brain as soluble macromolecules, then showing the tendency to form oligomeric, multimeric and fibrillar aggregates, thus triggering neurodegeneration. Soluble oligomers are now considered the main responsible for cognitive dysfunction, specially in the very early phases of the disease [2]. According to the amyloid cascade theory [3], the aggregation and accumulation processes of Aβ peptides end up with the formation of extracellular plaques that are considered the hallmarks of the disease. We first described a missense mutation in the alanine 673 residue of the amyloid precursor protein (APP), which corresponds to the second alanine of the amyloid Aβ A2V sequence, with dramatic impact on homozygous carriers [4]. More recently, Jonsson et al (2012) [5] reported a mutation on the same alanine residue (A673T) that protects against the onset and development of Alzheimer disease and age-related cognitive impairment. The complete mechanism of this protective effect is not yet understood, although some studies on different cell models suggest that this last variant reduces the BACE1-mediated processing of APP, then lowering the levels of Aβ production [5,6]. Differences in the fibrillogenic propensity of the mutated peptides have also been claimed, but results on Aβ A2T (both 1-40 and 1-42) are controversial, reporting either an effect on Aβ1-40_{A2T} kinetics of aggregation [7], or a reduced level in Aβ1-42_{A2T} aggregation but not in Aβ1-40_{A2T} [6]. We reported that the punctual mutation (A2V) increased the fibrillogenic properties of both Aβ1-40_{A2V} and Aβ1-42_{A2} [4,8]. These observations contribute to underlining the critical role played by the N-terminal Aβ region, which seems to affect the kinetics of oligomerization of peptides.

In the present work we were interested in clarifying whether a single amino acid substitution A-to-T or A-to-V in position 2 could cause the global reorganization of the peptide structure. To this regard, we observe that the controversial results for Aβ A2T were essentially obtained by the thioflavin T fluorescent dye method [6-7,9] that detects the presence of β-sheet structures then inferring fibrillation. Conversely, in this work we applied a more direct and multi-technique approach, using Static and Dynamic laser Light Scattering and Circular Dichroism. We also used the so called “depsi peptide method” for Aβ peptide synthesis, that enables obtaining seed-free batches of monomeric peptides [10-12].

We were able to compare in great detail the evolution from monomers toward fibrils of wild type Aβ WT sequence and of the mutated Aβ A2V and Aβ A2T, and to unravel the different nature of the oligomeric structures of Aβ peptides in the early stages of aggregation. We also compared the toxicity *in vitro*, on N2a cell lines, of the wild type peptide and the variants.

Finally, we also studied the interaction of Aβ A2V and A2T oligomers with model membranes using X-ray Scattering. With this technique one can observe the structural response of membranes to external stimulation. Soluble wild type Aβ oligomers are “membrane-active” species that can facilitate membrane puncturing and increase its permeability [13-15]. After interaction with the Aβ peptide, model membranes show structural rearrangement, with an expansion of the surface area

and an alteration of their microviscosity [16-18]. We also recently studied the interaction of the Aβ WT peptide with complex biomimetic membranes by Neutron Reflectometry [19] assessing how different stages of aggregation of the peptide result in different extent of interaction. Here we report that both mutated peptides induced changes in the structure of model membranes, revealing the Aβ interaction with the hydrophobic core of the lipid membranes.
The multi-technique approach may help in understanding how the various phenomena involved in Aβ production and aggregation concur in determining the occurrence and timing of the pathological or protecting route.

2. Materials and methods

2.1 Peptide synthesis and samples preparation

Aβ1-42 peptides were synthetized using depsipetide method as previously described [10-12]. Aβ1-42_{WT}, Aβ1-42_{A2V} and Aβ1-42_{A2T} (sequences in Supplementary Material) were stored in acidic solution (water:trifluoroacetic acid, 0.02%) at a concentration of ~200 μM. The depsi-peptide method allows to obtain a seed free batch, as much as possible near to monomeric condition. The method consists in introducing an O-acyl isopeptide structure between the Gly25–Ser26 residues, stable at acidic pH and able to inhibit the self-aggregation. On changing to basic pH (switching procedure), the peptide is converted into the Aβ1-42 native sequence. Before the switching procedure, to minimize the pre-aggregated species and to obtain the best reproducibility, peptides were dissolved in acidic solution (water:trifluoroacetic acid, 0.02%) at 1 mg/ml and ultracentrifuged o/n (at 55.000 rpm, 4°C) to obtain a seeds-free samples, filtered on a Microcon (centrifugal filter devices, c.o. 10 kDa, Millipore) and, finally, concentrated on a Microcon (centrifugal filter devices, c.o. 3 kDa, Millipore) up to a concentration ≥ 200 μM. The switching procedure of depsi-Aβ was carried out at basic pH, in particular a mix of sodium hydroxide (NaOH) and ammonium hydroxide (NH_4OH) (ratio 3:1) was added to the peptide solutions to obtain final concentration of hydroxyl group of 10 mM (final pH of ~10) and incubated on ice for 10-15 minutes.
Mixed model membranes for X-ray scattering investigation were prepared by dissolution of the desired lipids, dipalmitoylphoshatidylcholine (DPPC) and ganglioside (GM1), in appropriate organic solvent. After complete solvent evaporation under rotation, the lipid thin film was humidified and rehydrated (c = 20 mg/ml). Unilamellar vesicles formed spontaneously (DPPC:GM1 = 10:1.5 mol:mol).

2.2 BACE activity assay

BACE activity was carried out according to Ghosh & al. 2000 using as substrates the following three sequences: EVKMDAE (WT), EVKMDVE (A2V) and EVKMDTE (A2T) [20,21]. The BACE1 substrates were synthesized by solid-phase peptide synthesis on an automated synthesizer (Applied Biosystems 433A) using Fmoc-protected L-amino acid derivatives. The substrates were linked to a fluorescent dye (EDANS) on the glutammic acid in position 2 and to a quenching group (DABACYL) on the lysine in position 11. All peptides were purified in HPLC and their purity and identity were determined by MALDI-TOF analysis (model Reflex III, Bruker). BACE1 assay was carried out at 37ºC using 0,5 U of human recombinant BACE1 enzyme and different concentrations of substrate, 3.3, 6.6 and 10 μM, in 50 mM sodium acetate buffer (pH 4.5) in a final volume of 300 μl. Fluorescence was measured using a spectrophotofluorimeter (Perkin Elmer, Waltham, MA).

Wavelengths of excitation and emission were 336 nm and 493 nm, respectively. The kinetics were followed for 90 min.

2.3 Laser light scattering

Both Dynamic and Static Laser Light Scattering (DLS and SLS) techniques were used. Experiments were carried out on a non-commercial apparatus equipped with a laser (λ= 532 nm), a digital correlator, and a thermostated cell [22]. High sensitivity is reached with four optical channels at 90°, displaced 5° above or below the scattering plane, that allow independent parallel measurements of the intensity scattered from the same very dilute sample (about 0.1 mg/ml in the present work). Data reported in the Results were obtained by averaging the signal collected by all of the four independent optical channels.

The three peptides ($A\beta1\text{-}42_{WT}$, $A\beta1\text{-}42_{A2V}$ and $A\beta1\text{-}42_{A2T}$) were analyzed immediately after the switching procedure, described in 2.1, followed by dilution to the final concentration of 25 μM in phosphate buffer 50 mM, pH 7.4 at 22°C, by parallel and independent SLS and DLS. SLS average intensity depends on the molecular mass of particles in solution. So, the kinetics of aggregation of peptides was detected by acquiring the scattered intensity (SLS) for several days. The concentration being the same for all the samples and the measurements performed at the same temperature (22°C) with the same apparatus, differences in the scattered intensity could be directly related to differences in the number and molecular mass of the aggregates. Parallel measurement of the intensity correlation function (DLS) gave information on the translational diffusion coefficient of the particles and then, via the Stokes-Einstein equation, on the hydrodynamic radius of the aggregates. DLS data analysis was carried out using both the cumulants method, suitable to detect the evolution of the weight-average hydrodynamic size of particles in solution, and the NNLS method [23], suitable to determine their size distribution at different incubation times.

2.4 Circular Dichroism (CD)

Depsi peptides were switched as previously described and their initial secondary structures were determined at 4°C, immediately after dilution to the final concentration of 50 μM in phosphate buffer 50 mM, pH 7.4. Then, temperature was raised to 37°C and the samples were analyzed for 24 h in quiescent conditions (carrying out a scan every 30 minutes). CD spectra were recorded on a Jasco J-815 spectropolarimeter (Jasco, Easton, MD) from 200 to 260 nm (1.0-nm bandwidth and 0.1-nm resolution) using a 0.1 cm path length quartz cell (sensitivity = 0.1 deg, response = 4 s, scan speed = 50 nm/min, 5 accumulations). The spectrum of appropriate buffer was subtracted, and the resulting CD spectra of the samples were expressed as mean molar ellipticity (Φ). Deconvolution of the CD spectra was performed with the analysis program CONTIN [24] on an online server (DichroWeb).

2.5 Atomic Force Microscopy (AFM)

Depsi peptides were switched as previously described and diluted to the final concentration of 50 μM in phosphate buffer 50 mM, pH 7.4, then incubated in quiescent condition for 24 h. After incubation, all the samples were diluted to 5 μM with PBS 50 mM, then 20 μl were spotted onto freshly cleaved mica (Bruker AFM probes) at room temperature for five minutes and finally washed with 5 ml of milliQ water and dried under gentle nitrogen flow. AFM measurements were carried

out on a Multimode AFM with a Nanoscope V system operating in tapping mode, using standard antimony-doped silicon probes (T: 3.75 μm, L: 125 μm, W: 35 μm, k: 40 N/m, f_0: 300 kHz, Bruker AFM probes) with a scan rate in the 0.5-1.2 Hz range, proportional to the area scanned. In order to exclude the interference of possible artifacts, freshly cleaved mica and freshly cleaved mica soaked with 20 μl of PBS 50 mM, were also analyzed, as controls. All the topographic patterns were confirmed by measurements in a minimum of five different, well separated areas.

2.6 X-ray scattering (SAXS, WAXS)

Small angle X-ray scattering (SAXS) and wide angle X-ray scattering (WAXS) experiments were performed at the high-brilliance ID02 beamline of ESRF (Grenoble, France) in the region of momentum transfer $0.02 \leq q \leq 30$ nm^{-1}. Samples were put in plastic capillaries (KI-beam, ENKI) and mounted horizontally onto a thermostated multi-place sample holder, allowing for nearly simultaneous measurements on sample and reference cells. Very short exposure time was chosen (0.1 s), to avoid any radiation damage. The measured intensity profiles report the intensity of the scattered radiation as a function of the momentum transfer, q. To investigate a wide q-region, spectra relative to different q-ranges were joined, two for SAXS (with sample-to-detector distances of 1 m and 6 m) and one for WAXS, with an incident wavelength $\lambda = 0.1$ nm. Several spectra relative to the empty cells and the solvent were taken, carefully compared and subtracted from each sample spectrum.

2.7 In vitro toxicity assay

To test the neurotoxicity of $A\beta_{WT}$, $A\beta_{A2T}$ and $A\beta_{A2V}$ oligomers, the murine neuroblastoma N2a was used. To obtained soluble oligomers preparations, all depsi peptides after the switched procedure were diluted at 100 μM in PBS 50 mM and incubated for 18 h at 4°C. N2a cell line was grown in Dulbecco's Modified Eagle's Medium (DMEM) containing 4.5 g/l glucose (Lonza) supplemented with 10^4 U/ml penicillin/streptomycin (Gibco), 2 mM L-glutamine (Gibco) and 10% fetal calf serum (FCS, Lonza) at 37°C, in humidified atmosphere at 5% CO_2. Confluent cells were trypsinized (0.025%, Gibco), resuspended in DMEM containing 1% FCS to minimize cell growth and plated at the concentration of $2x10^4$ cells/ml in transparent, flat bottom 96-multiwell plates (Corning). Cells were treated 4 hours after plating by adding 10 μl of different oligomeric Aβ1–42 solutions to the medium, to the following final concentrations: 0.078 - 0.156 - 0.3125 - 0.625 - 1.25 - 2.5 – 5 - 7.5 and 10 μM. Cell viability was determined 72 hours after treatment using a MTT reduction assay (Sigma Aldrich) and expressed as percent of control treated cell (with phosphate buffered saline) by mean ± standard deviation of four replicates.

3. Results

3.1 Effect of mutation on the β-secretase activity.

We initially examined the effect of the mutations on the BACE1 activity. Results are reported in Figure 1 for three different concentrations of the substrates after 90 min incubation. It can be seen that the BACE1 activity is nearly the same in the presence of either the A2T or the WT mutations, while it is highly increased for the A2V variant, the corresponding peptide being more easily cleaved from the corresponding parent APP.

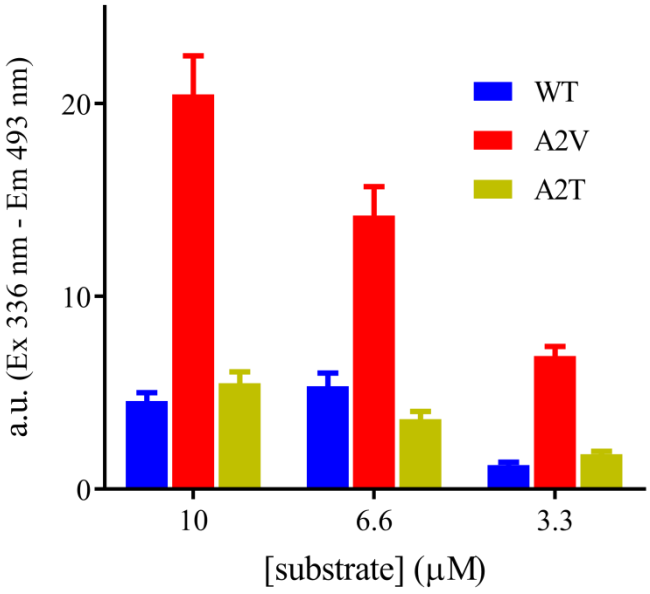

Figure 1. Recombinant β-secretase activity. Activity on APP carrying different mutations. (WT blue, A2V red, A2T green) determined with sequence-specific peptides containing the two reporter molecules EDANS and DABCYL. In the uncleaved form the fluorescent emission from EDANS is quenched by the physical proximity of the DABCYL moiety. Cleavage of the peptides by β-secretase physically separates the two reporters, enabling the release of the fluorescent signal at 493 nm. Concentrations of substrate: 3.3, 6.6 and 10 μM, in 50 mM sodium acetate buffer (pH 4.5). Delay from incubation: 90 min.

3.2 Aggregation

The aggregation propensity of the three Aβ peptides was investigated by laser light scattering. This technique readily reveals the emergence and growth of aggregates in solution, starting from monomers, as the measured scattered intensity (SLS) is proportional to the molecular mass of the scattering macromolecules. The depsi-peptide switching procedure was always used to avoid the presence of preformed seeds with high molecular mass, thus ensuring the monomeric starting point. The combination of depsi-peptide switching and radiation scattering observation has already proven to be well suited to follow the kinetics of aggregation of amyloidogenic peptides starting from monomeric condition [4,25,26]. In particular, in the case of Aβ1–42 peptides, a more pronounced propensity to aggregation was observed for the mutated A2V peptide as compared to the WT [8].

The early stages of aggregation are deeply influenced by several parameters, such as concentration and temperature. For this reason, in order to compare the effect of either A-to-V or A-to-T mutations on the aggregation pathway of Aβ, we applied the light scattering technique in the same experimental conditions to all systems. The aggregation was followed for at least 100 hours from switching, at 22°C on 25 μM peptide solutions in phosphate buffer 50 mM, pH 7.4. Parallel measurements of the intensity correlation function yielded the size distribution of particles in solution. Results obtained for the three systems are reported in Figure 2 for comparison.

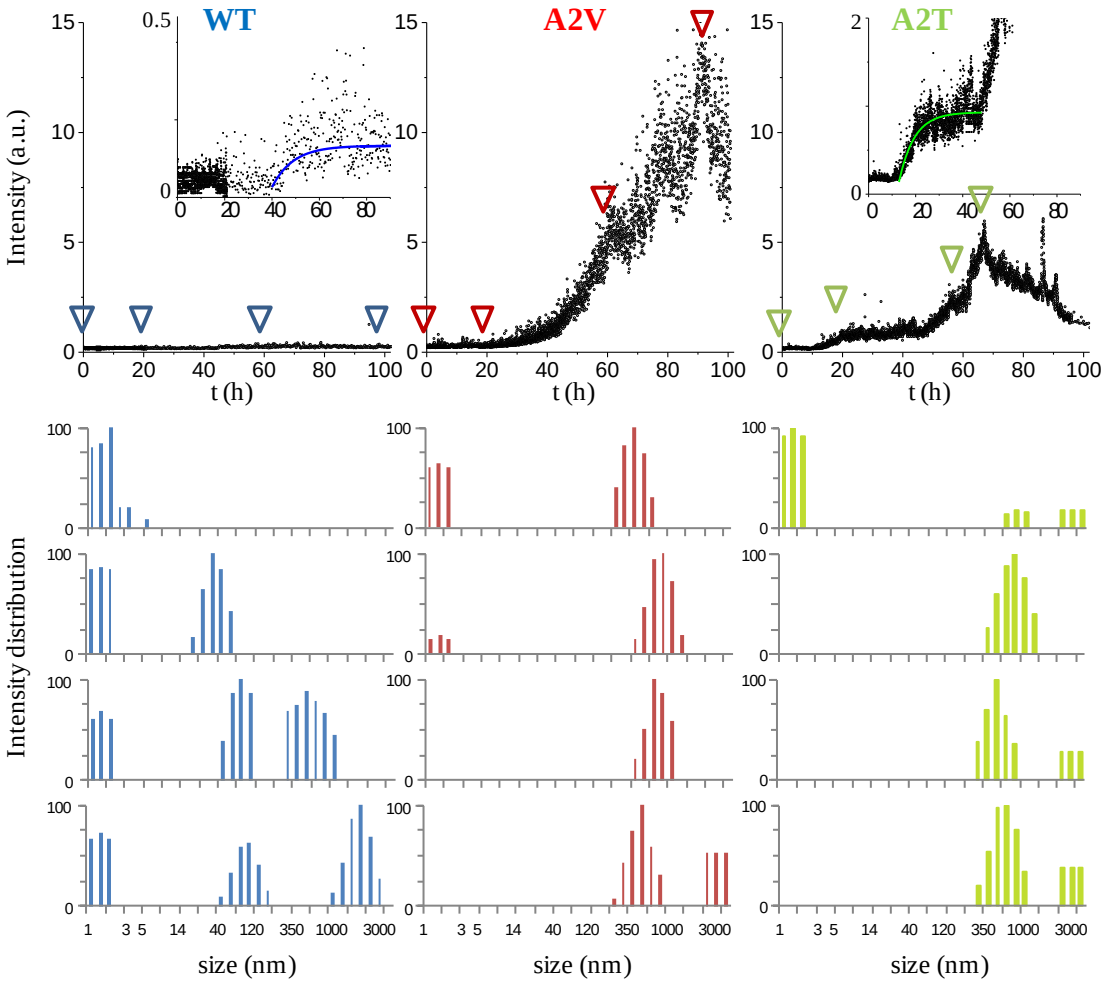

Figure 2. **Laser light scattering determinations**. *Top row*. SLS Scattered intensity as a function of delay from dissolution for Aβ1–42 WT, A2V, A2T, 25 μM at 22°C. The vertical scale is the same, so that the different extent of the scattered intensity growth can be appreciated. In the enlarged inserts, the fits of the observed kinetics, $I(t) = I_{final} (1 - e^{-t/\tau})$, where I_{final} is the asymptotic value of the scattered intensity growth and τ is the characteristic time. WT, blue line: $I_{final} = 0.08$, $\tau_{WT} = 9$ h; A2T, green line: $I_{final} = 0.78$, $\tau_{A2T} = 6.5$ h.
Following rows. DLS intensity-weighted size distribution of aggregates of the Aβ1–42 peptides (WT, blue; A2V, red; A2T, green), at different delays from dissolution, namely 0-1 h, 20 h, 60 h and final, as indicated in the top row by the arrows.

The initial intensity scattered from all samples was always very low, less than 1.5 times that of the pure solvent, as expected for very dilute solutions (about 0.1 mg/ml) of small particles. Data were obtained by averaging the signal collected by four different optical channels. The low scattered intensity confirmed that the peptides were present as monomers just after sample preparation. Looking at SLS results (Figure 2 first row), it is evident that the aggregation process for the three Aβ1–42 peptides was very different, both in the extent and in the kinetics. At a glance, $A\beta1–42_{WT}$ showed a definitely lower increase of the scattered intensity as compared to the two mutated peptides. $A\beta1–42_{A2V}$ displayed the highest intensity growth, even 100 times more than $A\beta1–42_{WT}$, while $A\beta1–42_{A2T}$ displayed an intermediate maximum value. Also SLS time evolution showed distinctive features for the three peptides. $A\beta1–42_{WT}$ aggregation started after a long lag time (40

h). Aβ1–42_{A2T}, after a shorter lag time (13 h), started a two-step aggregation process. The fitting curves reported in the inserts of Figure 2 were obtained by $I(t) = I_{final} (1 - e^{-t/\tau})$, where I_{final} is the asymptotic value of the scattered intensity growth and τ is the characteristic time, namely τ_{WT} = 9 h and τ_{A2T} = 6.5 h. Notably, the first step of Aβ1–42_{A2T} kinetics came to an end before the onset of Aβ1–42_{WT} aggregation.

To examine these differences in deeper detail, we compared DLS parallel results on the size distributions of the aggregates (*see Figure 2 following rows*). Data are reported as intensity-weighted size distributions at four different delays from dissolution, for each of the three peptides. At the beginning, monomers with size 2-3 nm were present in all systems, as the substantially predominant specie, > 80% relative intensity, corresponding to nearly 100% relative volume or number of particles.

For Aβ1–42_{WT}, at 20 h delay we detected the formation of intermediate aggregates of size 35 nm in coexistence with the population of monomers. Intermediate aggregates were few at this stage, as the intensity did not increase significantly. At 40 hours delay, a slight increase in intensity (*insert to first row-left panel)* was accompanied by the observation of two populations of aggregates with size ~60 nm and ~400 nm. The size of the largest aggregates slowly increased above 1000 nm, but seemingly their number remained very low, as the population of small monomers was still detectable after 100 h.

For Aβ1–42_{A2V}, aggregation started immediately as a unique process leading to the formation of an increasing number of large aggregates, ~500 nm in size. After 60 h monomers were no more detectable and at 90 h sedimentation of fibrils (size >2000 nm) occurred, as deduced by the final decrease of the scattered intensity (*first row-central panel*)

For Aβ1–42_{A2T}, , monomers disappeared to the benefit of the population of 500 nm (τ_{A2T} = 6.5 h) but in this case after a time lag of 13 hours. The number and the size of those aggregates reached a steady state (*insert to first row-right panel*), until, at 40 h delay, a second different process leaded to the formation of larger aggregates (fibrils of size >2000 nm) that, although fewer than in the case of Aβ1–42_{A2V}, underwent earlier sedimentation (t = 65 h).

The secondary structure of the Aβ peptides and the changes in their conformation due to peptide-peptide interactions were determined by CD. In the case of Aβ peptides, kinetics studies allow to follow the early changes of their secondary structure and in particular the detection of β-sheet formation. Aβ1–42 WT, A2V, A2T were analyzed immediately after switching and dilution to a final concentration of 50 μM at 37°C. Structural modifications were recorded for 24 hours with a scan every 30 minutes.

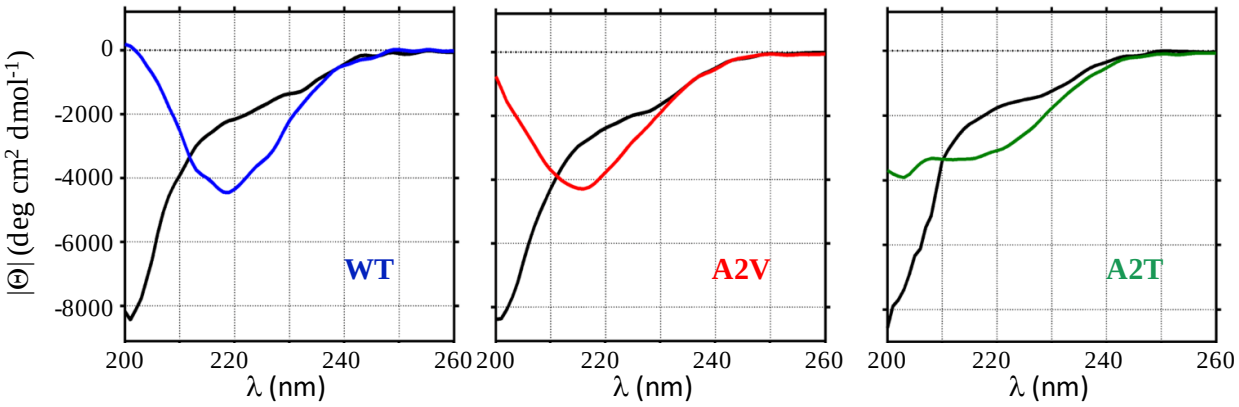

Figure 3. **Far-UV CD spectra of Aβ1-42$_{WT}$, Aβ1-42$_{A2V}$ and Aβ1-42$_{A2T}$.** Depsi peptides were switched to native Aβ1-42 sequences, diluted in 50 mM PBS buffer and immediately analyzed at 4°C (initial state, black lines). Temperature was increased to 37°C and the samples were incubated for 24 h in quiescent conditions (24 h, colored lines). Each spectrum corresponds at the mean of five accumulations. CD spectra were expressed as mean molar ellipticity.

Results are reported in Figure 3 at 0 h (black lines) and 24 h (colored lines). After dilution, all peptides displayed a predominant random-coil conformation (negative peak in the region 200 nm). The evolution of the secondary structure of the three peptides (reported in the Supplementary Material, Figure S1) was different. In particular, Aβ1–42$_{A2V}$ rapidly evolved to β-sheet, as already visible after 3 hours, confirming the effect of the A to V mutation in inducing swifter structural change towards the fibril-forming conformations. Table 1 reports the quantitative analysis obtained by deconvolution of the spectra collected after 24 h from dissolution. For Aβ1–42$_{A2V}$ the relative abundance of random-coil dropped down from 41.1% to 21.1%, while the β-sheet conformation (peak at 218 nm in Figure 3, red line) grew to 49.4%. Notably, the Aβ1–42$_{WT}$ peptide showed a slower kinetics, although reaching a quite similar distribution of secondary structures after 24 h at 37°C. Conversely, clear differences were detected for Aβ1–42$_{A2T}$. The initial distribution was nicely similar to the others, with a high content of random-coil, while after 24 h the fraction of random-coil conformation did not decrease dramatically, still remaining around 33.6%. Consistently, the fraction of β-sheet did not increase significantly, as visible in Figure 3 (peak at 218 nm, green line). Parallel examination of CD and light scattering results revealed that the different aggregation pathway observed for Aβ1–42$_{A2T}$ was accompanied by a different conformational evolution of the peptide. The soluble supramolecular aggregates formed by Aβ1–42$_{A2T}$ contained a lower fraction of β-sheet conformation.

	Aβ1–42 WT				Aβ1–42 A2V				Aβ1–42 A2T			
	α	βt	**β**	**coil**	α	βt	**β**	**coil**	α	βt	**β**	**coil**
0 h	2.9	21.0	**33.5**	**42.7**	2.1	23.9	**32.8**	**41.2**	2.2	23.7	**33.5**	**40.7**
24 h	7.9	22.3	**47.8**	**22.0**	7.2	22.1	**49.4**	**21.2**	7.8	23.4	**35.2**	**33.6**

Table 1. The content of secondary structures predicted by CD spectra using the CONTIN algorithm for Aβ1–42 WT, A2V, A2T (50 μM, 37°C). Fractional distribution (%) of different secondary structures, (α) α-helix, (βt) β-turn, (β) β-sheet, (coil) random-coil.

AFM was employed for morphological characterization of the 24-h-delay molecular assemblies of the three Aβ peptides present in the solutions used for CD analysis. The Aβ1-42$_{WT}$ sample was mainly composed by an abundant meshwork of mature protofibrillar structures with typical turn-loop, whereas the mutated peptides evolved in mature fibrillar structures, indicating higher fibrillogenic propensity. (Figure 4)

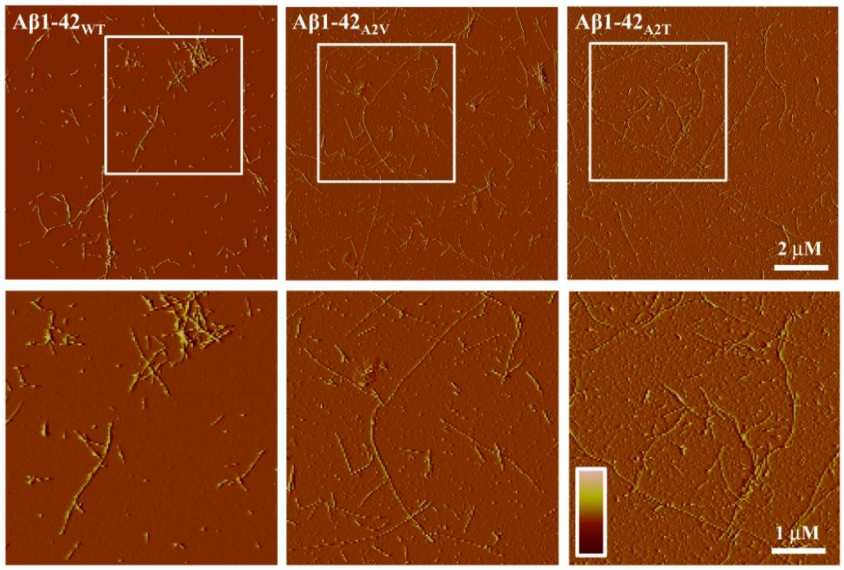

Figure 4. Analysis of Aβ1-42$_{WT}$, Aβ1-42$_{A2V}$ and Aβ1-42$_{A2T}$ in tapping mode atomic force microscopy (amplitude data). Aβ1-42 peptides switched were diluted to 50 μM in 50 mM phosphate buffer at 37°C in quiescent conditions and analyzed after 24 h after dilution to a final concentration of 5 μM. AFM images reported in Figure are representative of a minimum of five different, well separated areas. The scale bars correspond to an amplitude range of – 35 / + 60 mV for all panels.

3.3 Interaction with model membranes

To compare the propensity of the two mutated Aβ1–42$_{A2V}$, Aβ1–42$_{A2T}$ peptides to interact with membranes, we performed X-ray scattering experiments on model vesicles, containing DPPC phospholipid and GM1 ganglioside.

Closed unilamellar model membranes were prepared at 20 mg/ml of total lipid and then submitted to the interaction with mutated Aβ peptides (25 μM), at T = 50°C, well above the transition temperature of DPPC. Parallel Small and Wide Angle X-ray scattering measurements (SAXS and WAXS) were performed for the different systems. These techniques enable to obtain detailed information on the structure of the lipid bilayers constituting the model membranes.

All the recorded SAXS intensity profiles, reported in Figure 5, showed the typical features of closed unilamellar vesicles. Clearly, the spectra of the mixed systems (Aβ1–42$_{A2V}$ red points, Aβ1–42$_{A2T}$ green diamonds) were very similar to each other and both different from the one of the naked membrane (black triangles), indicating that interaction occurred between both peptides and the model membrane.

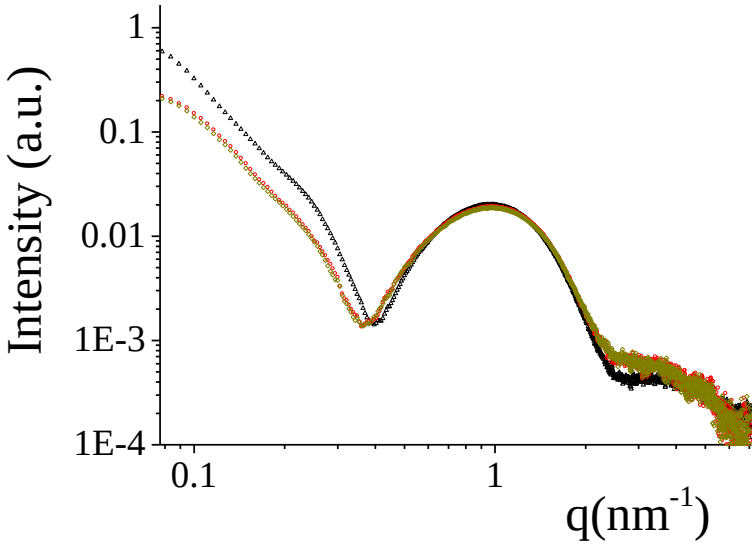

Figure 5. Small angle X-ray (SAXS). Spectra of model membrane solutions (DPPC:GM1 = 10:1.5) naked (black) and in presence of Aβ1–42$_{A2V}$ (red) and Aβ1–42$_{A2T}$ (green) peptides.

Parallel measurements in the WAXS spectral region, corresponding to distances typical of the local scale, confirmed this finding. As shown in Figure 6, the intensity peak for the naked membrane was q_{peak}= 14.8, corresponding to a mean distance d = 0.424 nm between lipid chains in the fluid phase. In the mixed systems the sharpness of the WAXS peak was reduced and its position was moved to lower q values, indicating that the presence of Aβ1–42 peptides induced a higher degree of disorder in the packing of the lipid chains within the membrane core. The same disordering effect could be inferred from the observed modification of the SAXS spectra shown in Figure 5.

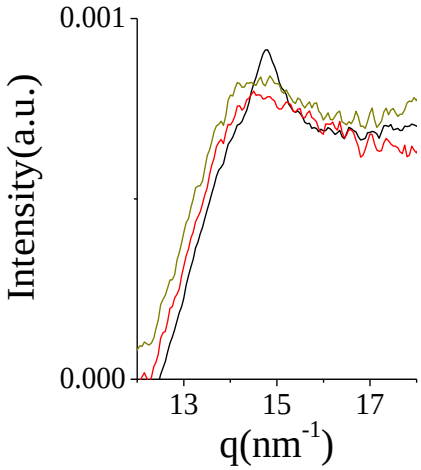

Figure 6. Wide angle X-ray (WAXS). Spectra of model membrane solution (DPPC:GM1 = 8:2) naked (black) and in presence of Aβ1–42$_{A2V}$ (red) and Aβ1–42$_{A2T}$ (green) peptides. Peak at q_{peak} = 14.8 nm^{-1} (black).

3.4 Toxicity

The cell viability of the neuroblastoma N2a after treatment with various concentrations of Aβ1-42_{WT}, Aβ1-42_{A2V} and Aβ1-42_{A2T} peptides was assessed. Figure 7 reports the cell viability 72 hours post administration of the different oligomeric peptides solutions in the concentration range 0.078 - 10 µM. The dose corresponding to 50% cell viability (EC50) were, 5 µM for WT, 1.05 µM for A2V and 2.5 µM for A2T. Therefore the toxicity for the three peptides could be ranked as Aβ1-42_{A2V} > Aβ1-42_{A2T} > Aβ1-42_{WT}.

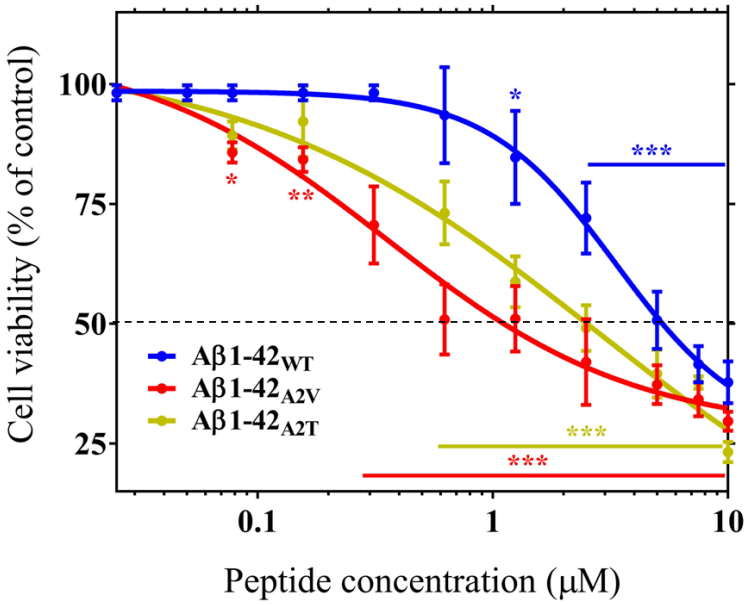

Figure 7. Neurotoxicity of Aβ1-42_{WT}, Aβ1-42_{A2V} and Aβ1-42_{A2T} oligomers. N2a cell viability after treatment with oligomers preparations at different concentrations (0.078-0.156-0.3125-0.625-1.25-2.5-5-7.5-10 µM) for 72 hours. Each point was mean ± standard deviation of four replicates, *p<0.05, **p<0.01, ***p<0.001 versus control (phosphate buffered saline), one-way ANOVA followed by Tukey's post hoc test. A horizontal dotted line marks the EC50 values.

4. Conclusions

We investigated the effects of punctual A-to-V and A-to-T mutations in position 673 of the amyloid precursor protein APP, in the N-terminus region, corresponding to position 2 of the Aβ1–42 peptide, on its aggregative properties and on its propensity to interact with membranes. Those mutations have opposite effects on the onset of AD, A-to-V inducing early onset of AD in the homozygous, while A-to-T preventing the pathology. Concerning the Aβ peptide production by β-secretase activity, we found that the A2V mutation enhanced APP processing, while the A2T mutation resulted in similar level of Aβ production as compared to the wild type. Still we found that this is not the only difference. We applied a multi-technique approach to study the structural and morphological features of the three Aβ peptides on different length-scales.

We applied static and dynamic laser light scattering techniques and CD to study the aggregation process of Aβ1–42_{WT}, Aβ1–42_{A2V} and Aβ1–42_{A2T} in the early stages. These correspond to the soluble-oligomers/structured-oligomers regime, where aggregates are claimed to be essential for the noxiousness in vivo and then for the onset and the advancement of the disease. We took advantage

of the so called “depsi peptide method” for Aβ peptide synthesis, that enables obtaining seed-free batches of monomeric peptides.

Comparative results indicated distinctive pathways of monomers aggregation that differed in the kinetics and the extent of the process, in the size of aggregates, in the evolution of the secondary structure of the peptides. This means that at a given concentration, at the same delay from production within a certain time lag, the three peptides display a different propensity to establish and stabilize interactions with similar molecules. This suggests that oligomeric species with different reactivity towards their surrounding medium may occur, with different outcomes.
Notably, $A\beta1–42_{WT}$ had the lowest propensity for aggregation, and in fact monomers were still observed at long delay from dissolution.
A-to-V mutation significantly increased the number and size of $A\beta1–42_{A2V}$ aggregated structures, leading to fibril formation. Accordingly, the secondary structure of the mutated $A\beta1–42_{A2V}$ peptide evolved faster to β-sheet conformation.
The behavior of $A\beta1–42_{A2T}$ was complex. A double-step kinetics led to the formation of intermediate aggregated structures before the appearance of a small number of fibrils, In parallel we also observed a slower folding kinetics: the distribution of secondary structures did not evolve rapidly towards an increasing amount of β-sheet. Thus $A\beta1–42_{A2T}$ aggregates were different from the usual pre-fibrillar ones observed in $A\beta1–42_{A2V}$, on different length-scales. The present findings agree with recent studies on monomers conformations [27] showing that the A-to-T mutation can dramatically alter the β-hairpin population and switch the equilibrium towards alternative structures. Moreover the observed time evolution of the collection of aggregates suggests that the intermediate aggregates did not evolve simultaneously towards the progressive formation of pre-fibrillar and fibrillar structures, but spare fibrils were formed randomly in solution. These fibrils immediately precipitated, as observed by laser light scattering, and were therefore no longer present in the solution to give the characteristic contribution to CD spectra. Early spare fibril sedimentation could also have affected the controversial results obtained by thioflavin T fluorescent dye method [6-7,9], that follows the fibrillation process by detecting the β-sheet signal.
Both $A\beta1–42_{A2V}$ and $A\beta1–42_{A2T}$ peptides had higher toxicity than $A\beta1–42_{WT}$. The dose response curve on neuroblastoma N2a cells viability indicated $A\beta1\text{-}42_{A2V}$ was the most toxic, with an onset of effectiveness and 50% cell viability at 72h at the lower dose.
Finally, we directly observed the interaction of $A\beta1–42_{A2V}$ and $A\beta1–42_{A2T}$ peptides with model membranes, at early stages of aggregation. Both peptides had a propensity to interact with membranes, leading to a decrease in the lipid core density and an increase in the disorder of the chains packing.

Acknowledgments

We are grateful to Ada Deluigi and Leilei Zhang for their support in the experiments.
We are grateful to ID02 beamline staff and T. Narayanan at the ESRF (Grenoble, France) for their technical assistance, Flamma Spa, Bergamo, Italy for the kind gift of Fmoc amino acids. The authors also acknowledge the Fondazione Sacchetti for the support for this study.

Supplementary material

Sequences of Aβ1–42 peptides.
Time evolution of far-UV CD spectra of Aβ1-42$_{WT}$, Aβ1-42$_{A2V}$ and Aβ1-42$_{A2T}$.

References

[1] D.H. Small, Roberto Cappai, Alois Alzheimer and Alzheimer's disease: a centennial perspective *J. of Neurochemistry* 99 (2006) 708–710.

[2] T.E. Golde, D. Dickson, M. Hutton, Filling the Gaps in the Aβ Cascade Hypothesis of Alzheimer's Disease *Curr Alzheimer Res* 3(5) (2006) 421-430.

[3] J. Hardy, D. J. Selkoe, The amyloid hypothesis of Alzheimer's disease: progress and problems on the road to therapeutics. *Science* 297 (2002) 353–356.

[4] G. Di Fede, M. Catania, M. Morbin, G. Rossi, S. Suardi, G. Mazzoleni, M. Merlin, A. R. Giovagnoli, S. Prioni, A. Erbetta, C. Falcone, M. Gobbi, L. Colombo, A. Bastone, M. Beeg, C. Manzoni, B. Francescucci, A. Spagnoli, L. Cantù, E. Del Favero, E. Levy, M. Salmona, F. Tagliavini, A recessive mutation in the APP gene with dominant-negative effect on amyloidogenesis *Science* 323 (2009) 1473-1477.

[5] T. Jonsson, J.K .Atwal, S. Steinberg, J. Snaedal, P.V. Jonsson, S. Bjornsson, H. Stefansson, P. Sulem, D. Gudbjartsson, J. Maloney, K. Hoyte, A. Gustafson, Y. Liu, Y. Lu, T. Bhangale, R.R. Graham, J. Huttenlocher, G. Bjornsdottir, O.A. Andreassen, E.G. Jönsson, A. Palotie, T.W. Behrens, O.T. Magnusson, A. Kong, U. Thorsteinsdottir, R.J. Watts, K. Stefansson, A mutation in APP protects against Alzheimer's disease and age-related cognitive decline *Nature* 488(7409) (2012) 96-99.

[6] J.A. Maloney, T. Bainbridge, A. Gustafson, S. Zhang, R. Kyauk, P. Steiner, M. van der Brug, Y. Liu, J. A. Ernst, R. J. Watts, J. K. Atwal, Molecular Mechanisms of Alzheimer Disease Protection by the A673T Allele of Amyloid Precursor Protein *JBC* 289(45) (2014) 30990–31000.

[7] I. Benilova, R. Gallardo, A. A. Ungureanu, V. Castillo Cano, A. Snellinx, M. Ramakers, C. Bartic, F. Rousseau, J. Schymkowitz, B. De Strooper, The Alzheimer Disease Protective Mutation A2T Modulates Kinetic and Thermodynamic Properties of Amyloid-β (Aβ) Aggregation *J. Biol. Chem.* 289 (2014) 30977-30989.

[8] M. Messa, L. Colombo, E. Del Favero, L. Cantù, T. Stoilova, A. Cagnotto, A. Rossi, M. Morbin, G. Di Fede, F. Tagliavini, M. Salmona, The peculiar role of the A2V mutation *in* Aβ1-42 molecular assembly *JBC* 289 (2014) 24143-24152.

[9] B. Murray, M. Sorci, J. Rosenthal, J. Lippens, D . Isaacson, P. Das, D. Fabris, S. Lι, G. Belfort, A2T and A2V A□ peptides exhibit different aggregation kinetics, primary nucleation, morphology, structure, and LTP inhibition Proteins 2016; 84:488–500.

[10] A. Taniguchi, Y. Sohma, Y. Hirayama, H. Mukai, T. Kimura, Y. Hayashi, K. Matsuzaki, Y. Kiso, "Click peptide": pH-triggered in situ production and aggregation of monomer Abeta1-42. *Chembiochem* 10 (2009)710-715.

[11] I. Coin, The depsipeptide method for solid-phase synthesis of difficult peptides. *J Pept Sci* 16 (2010) 223-230.

[12] M. Beeg, M. Stravalaci, A. Bastone, M. Salmona, M. Gobbi, A modified protocol to prepare seed-free starting solutions of amyloid-β (Aβ)1-40 and Aβ1-42 from the corresponding depsipeptides. *Anal Biochem* 411 (2011) 297-299.

[13] R.H. Ashley, T.A. Harroun, T. Hauss, K.C. Breen, J.P. Bradshaw, Autoinsertion of Soluble Oligomers of Alzheimer's Aβ(1-42) Peptide into Cholesterol-containing Membranes Is Accompanied by Relocation of the Sterol Towards the Bilayer Surface. *BMC structural biology* 6 (2006) 21-32.

[14] R. Kayed, Y. Sokolov, B. Edmonds, T.M. Mcintire, S.C. Milton, E. Hall, C.G. Glabe, J.E. Hall, Permeabilization of Lipid Bilayers Is a Common Conformation-dependent Activity of Soluble Amyloid Oligomers in Protein Misfolding Diseases *JBC* 279 (2004**)** 46363–46366.
[15] T.L. Williams, L.C. Serpell, Membrane and surface interactions of Alzheimer's A*β* peptide – insights into the mechanism of cytotoxicity. *Febs J.* 278 (2011) 3905-3917.
[16] C.M.Yip, A. Darabie, J. McLaurin, Abeta42-peptide Assembly on Lipid Bilayers. *J. molecular biology* 318 (2002) 97–107.
[17] M. C. Vestergaard, M. Morita, T. Hamada, M. Takagi, Membrane Fusion and Vesicular Transformation Induced by Alzheimer's Amyloid Beta. *BBA* 1828 (2013)1314–1321.
[18] S.V. Chochina, N.A. Avdulov, U. Igbavboa, J.P. Cleary, E.O. O'Hare, W.G. Wood, Amyloid Beta-peptide1-40 Increases Neuronal Membrane Fluidity: Role of Cholesterol and Brain Region. *Journal of lipid research* 42 (2001) 1292–1297.
[19] V. Rondelli, P. Brocca, S. Motta, M. Messa, L. Colombo, M. Salmona, G. Fragneto, L. Cantu', E. Del Favero. Amyloid-β Peptides in interaction with raft-mime model membranes: a Neutron Reflectivity insight. Nature Sci.Reports (2016)
[20] A.K. Ghosh, D. Shin, D. Downs, G. Koelsch, X. Lin, J. Ermolieff, J.Tang, Design of Potent Inhibitors for Human Brain Memapsin 2 (β-Secretase) *J Am Chem Soc* 122 (2000) 3522–3523.
[21] J. Lamar, J. Hu, A.B. Bueno, H.C. Yang, D. Guo, J.D. Copp, J. McGee, B. Gitter, D. Timm, P. May, J. Mccarthy, S.H. Chen, Phe*-Ala-based pentapeptide mimetics are BACE inhibitors: P2 and P3 SAR *Bioorg Med Chem Lett* 14 (2004) 239–243.
[22] P. Lago, L. Rovati, L. Cantù, M. Corti A quasielastic light scattering detector for chromatographic analysis, *Review of Scientific Instruments* 64 (1993) 1797-180.
[23] C.L. *Lawson, R.J. Hanson (1995) Solving Least Squares Problems*, Vol 15, SIAM, Philadelphia, PA
[24] N. Sreerama and R. W. Wood, Estimation of Protein Secondary Structure from Circular Dichroism Spectra: Comparison of CONTIN, SELCON, and CDSSTR Methods with an Expanded Reference Set, *Analytical Biochemistry* 287(2000) 252–260.
[25] M. Stravalaci, A. Bastone, M. Beeg, A. Cagnotto, L. Colombo, G. Di Fede, F. Tagliavini, L. Cantù, E. Del Favero, M. Mazzanti, R. Chiesa, M. Salmona, L. Diomede, M. Gobbi, Specific reco*gnition of biologically* active amyloid-β oligomers by a new surface plasmon resonance-based immunoassay and an in vivo assay in Caenorhabditis elegans. *J Biol Chem* 287 (2012) 27796-27805.
[26] L. Diomede P. Rognoni, F. Lavatelli, M Romeo, E. Del Favero, L. Cantù, E. Ghibaudi, A. di Fonzo, A. Corbelli, F. Fiordaliso, G. Palladini, V. Valentini, V. Perfetti, M. Salmona, G. Merlini, A *Caenorhabd*itis elegans-based assay recognizes immunoglobulin light chains causing heart amyloidosis. *Blood* 123(23) (2014)3543-52.
[27] P. Das, B. Murray, G. Belfort, Alzheimer's Protective A2T Mutation Changes the Conformational Landscape of the Ab1–42 Monomer Differently Than Does the A2V Mutation Biophysical Journal 108 (2*015) 738–747*.